JOURNAL OF MATERIALS SCIENCE **39** (2004) 6253–6256

Low and high-cycle fatigue properties of 12Cr-2W ferritic steel at high temperature

K. KOBAYASHI
Materials Information Technology Station, National Institute for Materials Science (MITS/NIMS), 1-2-1 Sengen, Tsukuba, Ibaraki 305-0047, Japan
E-mail: KOBAYASHI.Kazuo@nims.go.jp

K. YAMAGUCHI, M. KIMURA, M. HAYAKAWA
MITS/NIMS, 1-2-1 Sengen, Tsukuba, Ibaraki 305-0047, Japan

Axial strain- and load-controlled fatigue tests of a 12Cr-2W ferritic heat resisting steel were performed at high temperatures to obtain a continuous fatigue life curve (S-N curve) over a wide range from 10^2 to 10^9 cycles using load-alignment adjusted testing machines. When the stress amplitude (σ_a) in the S-N curve was normalized by tensile strength (σ_B), the ratio (σ_a/σ_B) decreased to below 0.5 over 10^6 cycles at 650°C. The reason was considered to be caused by internal fractures over 10^6 cycles at 650°C.

1. Introduction

9–12%Cr ferritic steel has a lower thermal expansion coefficient and a higher creep rupture strength than austenitic stainless steel. A tungsten-strengthened 12Cr-2W ferritic heat-resistant steel has been developed recently and is now in use for main steam pipes and headers in power plants [1–5].

Fossil fuel power plants operate under daily start-up and shut-down conditions, and temperatures also fluctuate during operation, resulting in considerable thermal stress being applied to their components. The flow of steam and water causes vibration of pipes and tubes. The temperature changes due to the start-up and shut-down operation and operational fluctuations cause strain-controlled low-cycle (high and low strain) fatigue, and the vibration of the components causes load-controlled ultra high-cycle fatigue.

The purpose of this study was to investigate the fatigue properties of the new 12Cr-2W steel over a wide range from low-cycle to ultra high-cycles regions. For low-cycle fatigue, a strain-controlled test was conducted in the range from 10^2 to 10^7 cycles. For high-cycle fatigue, a load-controlled test was conducted in the range from 10^4 to 10^9 cycles. Finally, we attempted to make a single universal S-N fatigue curve from 10^2 to 10^9 cycles by combining both sets of data.

2. Experimental procedure

2.1. Materials

The chemical composition and heat-treatment conditions of the material used in this study are shown in Table I. Fig. 1 shows the optical microscope image of a 5%-nital etched-surface. The material has a tempered martensitic microstructure, and the prior austenite grain size is about 30 μm in diameter. The material was hot-rolled plate with a thickness of 28 mm. The test specimen was machined along the rolling direction of the plate. The tensile strength is shown in Table II.

2.2. Testing condition

The fatigue specimen was a smooth cylinder with a diameter of 5 or 10 mm depending on the testing machine's capacity. The surfaces of the fatigue specimens were, however, identical and finished by polishing finally with 600-grit SiC paper.

For axial strain-controlled low-cycle fatigue tests, a digitally controlled hydraulic fatigue-testing machine was used with a load capacity of $\pm$100 kN. The controlled-strain wave shape was triangular, and the strain rate was 10^{-3} or 10^{-2}/s. Testing temperatures were room temperature (RT), 400, 600, 650 and 700°C at a strain rate of 10^{-3}/s, and the tests were conducted up to 10^6 cycles. At 650°C the tests were conducted at a strain rate of 10^{-2}/s up to 10^7 cycles. It takes three months to run the test up to 10^6 cycles under 10^{-3}/s. However, fatigue endurance limit dose not appear at the 10^6 cycles or 10^7 cycles.

For axial load-controlled high-cycle fatigue, a high frequency hydraulic testing machine with a voice-coiled servo-valve was used. Its maximum frequency was 1000 Hz under a $\pm$10 kN. Its testing temperatures were RT, 400 and 650°C at a frequency of 1–800 Hz. The stress ratio ($\sigma_{min}/\sigma_{max}$) was -1, that is tension-compression conditions.

Both the testing machines have an adjusting jig for loading alignment. For heating the specimen, an electric resistance furnace and an induction furnace, respectively, were used for the strain-controlled and load-controlled fatigue testing machines.

TABLE I Chemical composition and heat treatment conditions of the material

Element	C	Si	Mn	P	S	Cu	Ni	Cr	Mo	V	Nb	W	Al	N
Composition	0.12	0.28	0.61	0.02	0.001	0.97	0.34	10.5	0.36	0.21	0.06	2.05	0.01	0.07

Processing & thermal history.
Hot rolled 1050°C/1.7 h air cooled (normalized); 770°C/6 h air cooled (tempered).

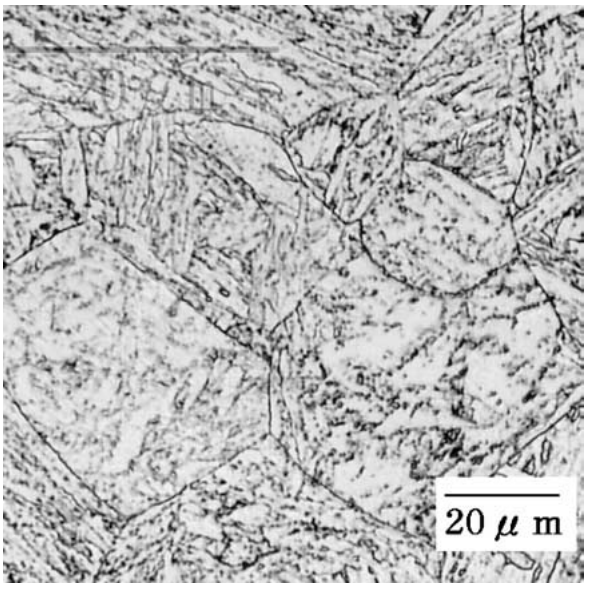

Figure 1 Microstructure of the material used.

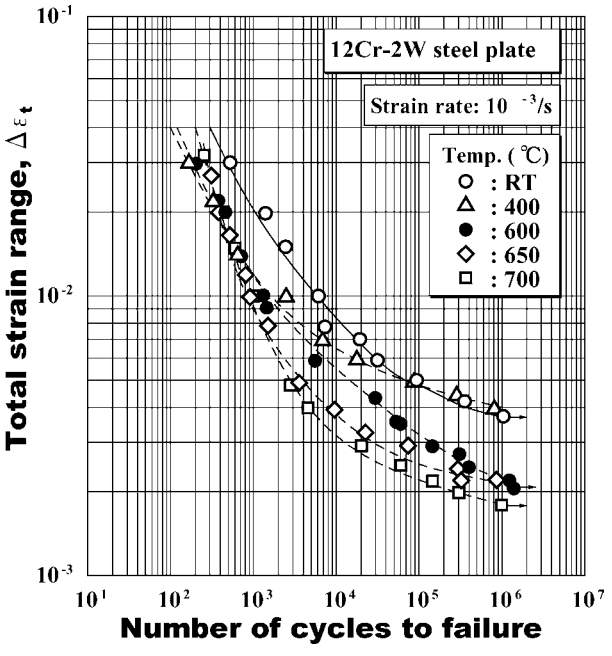

Figure 2 Fatigue life curves for tested temperatures.

3. Results

3.1. Strain-controlled low-cycle fatigue property

The test results at a strain rate of 10^{-3}/s are shown in Fig. 2. The arrows in the figure denote that the specimen did not fail. At each temperature, a smooth fatigue life curve (S-N curve) with minimal scatter was obtained over a wide range from 10^2 to 10^6 cycles.

Fig. 3 shows the data for conventional ferritic steels (Mod.9Cr-1Mo [5] and SCMV4 (2.25Cr-1Mo) [6]), an austenitic stainless steel (316FR [7]) and this experimental material at 600°C. The latter material is superior to conventional ferritic steels, and it has minimal scatter over a wide spread of data from 10^2 to 10^6 cycles. As for austenitic 316FR steel, its data are almost the same as this 12Cr-2W steel in the low-cycle region, but in the high-cycle region 316FR is superior to our experimental material. It should be noted that the high-cycle fatigue strength of ferritic steels may be lower than in austenitic steel, although the thermal expansion coefficient of ferritic steels is lower than that of austenitic steel. Acquiring competitive data in the high-cycle region is increasingly necessary for the design of high temperature components.

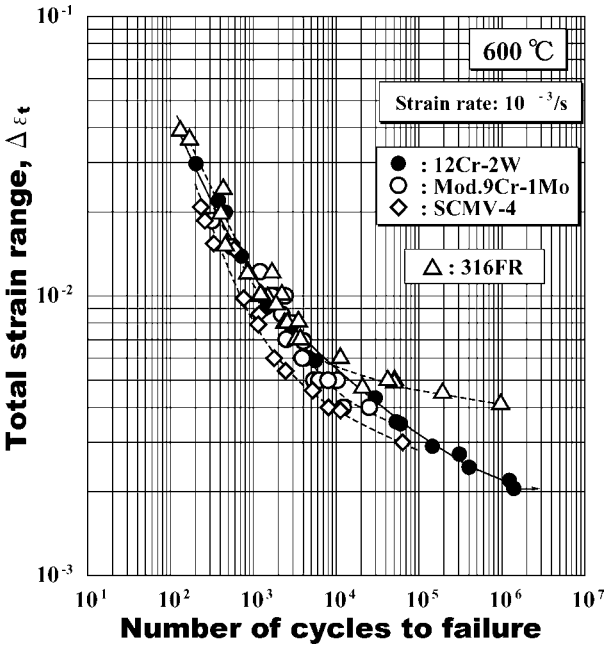

Figure 3 Comparison of fatigue data obtained in this study and references.

TABLE II Mechanical properties of the material

Temperature (°C)	0.2% proof stress (MPa)	Tensile strength (MPa)	Elongation (%)	Reduction of area (%)
RT	540	725	22	64
400	427	578	16	54
600	283	362	30	86
650	199	285	34	91
700	125	207	37	95

Fig. 4 shows the data at 650°C under a strain rate of 10^{-2}/s. The total strain range was divided into the plastic strain range ($\Delta\varepsilon_p$), and the elastic strain range ($\Delta\varepsilon_e$). Generally, the relationship between the plastic strain range and the fatigue life is linear in log-log plots,

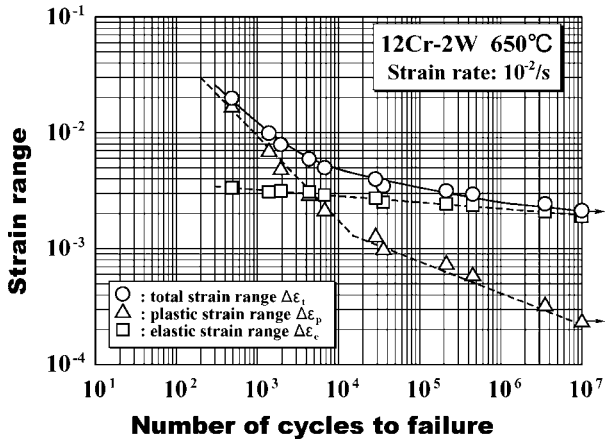

Figure 4 Relationship between plastic-strain range, elastic-strain range, total-strain range and fatigue life.

and is called a Manson-Coffin relationship.

It is written by Equation 1.

$$\Delta\varepsilon_{\mathrm{p}} \cdot N^{\alpha} = A \tag{1}$$

The relationship between the elastic strain range and the fatigue life is written by Equation 2.

$$\Delta\varepsilon_{\mathrm{e}} \cdot N^{\beta} = B \tag{2}$$

where α, A, β and B are material constants, and N is the number of cycles to failure.

In Fig. 4, however, the relationship between $\Delta\varepsilon_{\mathrm{p}}$ and N has an inflection at around 10^4 cycles. The material constants are given in Table III, especially α and β mean the slopes in Fig. 4.

The same inflection was observed at 600, 650 and 700°C under 10^{-3}/s, but not at RT or 400°C. At present the mechanism of this phenomenon, seen only at high temperatures, is not known, so extensive data for various kinds of materials up to the high-cycle region is needed.

3.2. Load-controlled high-cycle fatigue property

Fig. 5 shows the results of load- and strain-controlled fatigue tests at RT, 400 and 650°C. The stress amplitude in Fig. 5 is half the stress range at approximately half the number of cycles to failure in the case of the strain-controlled tests. At RT and 400°C no frequency effect is observed between 1 and 800 Hz, and between 0.01 and 800 Hz, respectively. At 650°C, on the other hand, a frequency effect is observed between 10^{-3} and 10^{-2}/s.

TABLE III Values of the material constants in Equations 1 and 2

Material constants in Equation 1 (until 10^4 cycle)		Material constants in Equation 1 (beyond 10^4 cycle)		Material constants in Equation 2 (until 10^7 cycle)	
A	α	A	α	B	β
1.97	0.782	0.0192	0.272	0.00471	0.055

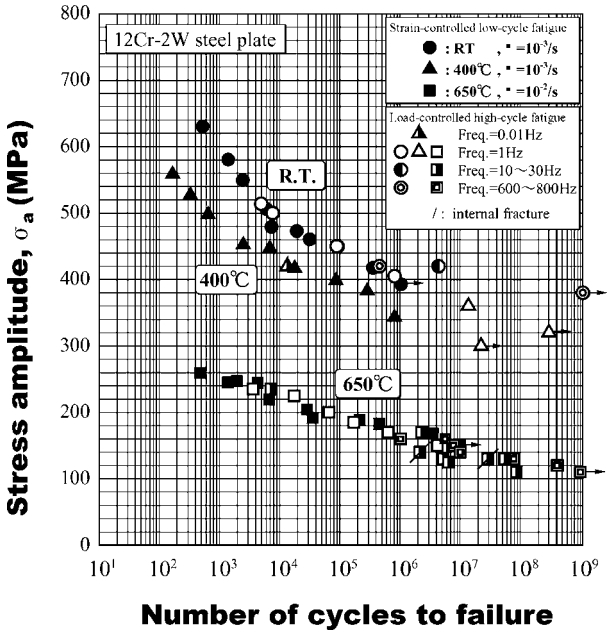

Figure 5 S-N curves of strain- and load-controlled fatigue tests.

However, between 10^{-2}/s and 1–800 Hz, very little frequency effect is observed, as shown in Fig. 5. The strain rate of 10^{-2}/s corresponds to a frequency of about 0.2–20 Hz, depending on the strain range. In Fig. 5, the "/" symbol on the data at 650°C indicates that the fracture mode is internal, i.e., a fish-eye fracture. An example is shown in Fig. 6. X-ray diffraction analysis revealed the inclusion to be aluminum oxide. In this material there were only a few specimens that clearly showed internal fracture; they had all been tested under load-controlled conditions at 650°C. The mechanism of fatigue fracture in the high-cycle region will be discussed in the next section.

4. Discussion

Fig. 7 shows an S-N curve normalized by tensile strength at each temperature. Generally, the fatigue limit (the fatigue strength at 10^7 cycles or 2×10^7 cycles) is expressed as half the tensile strength, such as $\sigma_{\mathrm{w}} = 0.5\sigma_{\mathrm{B}}$, where σ_{w} is the fatigue limit and σ_{B} is the tensile strength [8, 9]. In this case, the fracture mode is generally a surface fracture. The surface fracture is normal for a fatigue fracture mode. At RT and 400°C, this material has a fatigue limit of approximately half the tensile strength, and shows a surface fracture mode even in load-controlled high-cycle fatigue tests, as shown in Fig. 7. On the other hand, at 650°C, the normalized stress amplitudes over 10^6 cycles are below 0.5. Some specimens showed internal fractures, as shown in Fig. 7. The decrease in fatigue strength in the high-cycle region is considered to be caused by internal fractures. Because the fracture mode of some specimens was clearly internal, as shown in Fig. 6, although we could not determine the fracture modes of all the specimens as internal over 10^6 cycles. It was difficult to determine the fracture mode because the fracture surfaces tested at 650°C were covered with a thick oxide film.

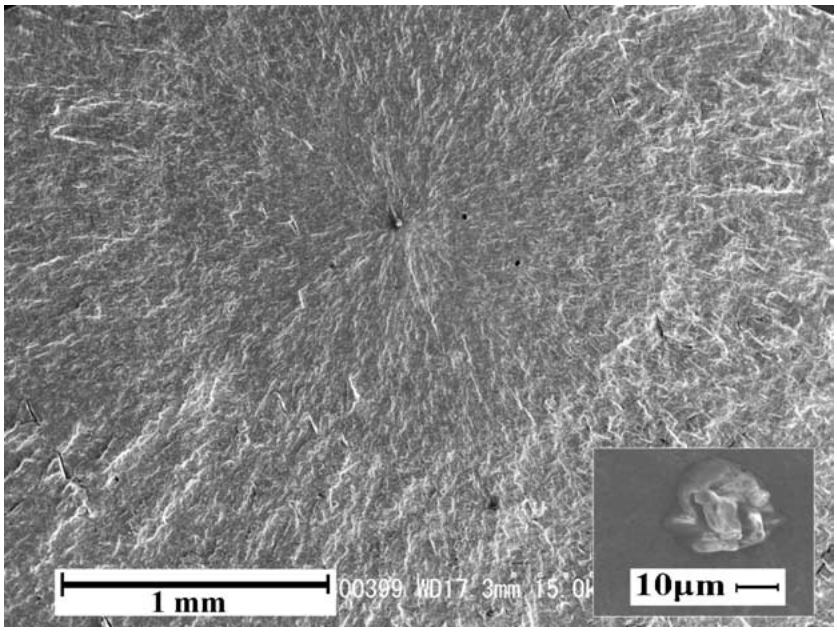

Figure 6 Typical internal fracture surfaces at 650°C over 10^6 cycles.

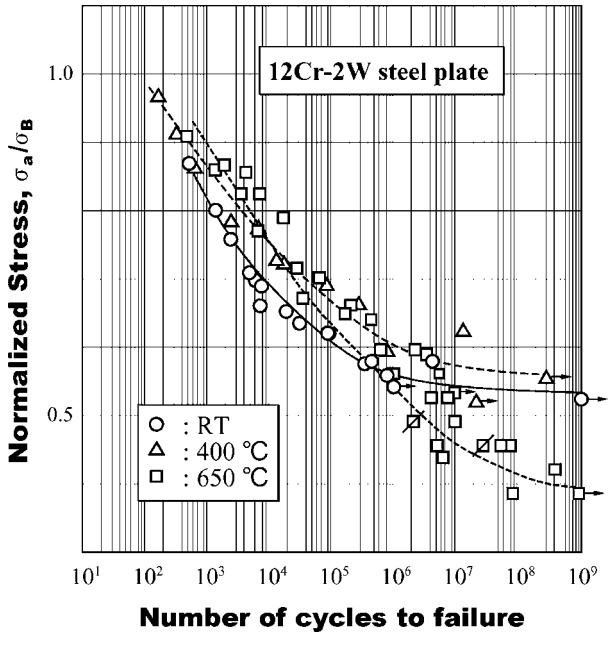

Figure 7 Normalized S-N curves by tensile strength.

5. Conclusions

The high temperature fatigue properties of 12Cr-2W steel were investigated by means of axial strain- and load-controlled tests over a wide range from 10^2 cycles to 10^9 cycles. The following conclusions were obtained.

1. The fatigue life curves obtained under strain-controlled fatigue tests were smooth in the range from 10^2 to 10^7 cycles and showed only limited scatter.

2. The Manson-Coffin relationship (plastic strain range vs. fatigue life) showed an inflection in the high-cycle region at temperatures over 600°C.

3. By combining both the data of strain- and load-controlled tests, we were able to assemble a universal S-N curve from 10^2 cycles to 10^9 cycles at RT, 400 and 650°C.

4. When the amplitude in the S-N relationship was normalized by tensile strength, the normalized fatigue strength at 650°C in the high-cycle region fell to below 0.5. The decrease was considered to be caused by internal fractures at over 10^6 cycles at 650°C.

References

1. ASME Boiler and Pressure Vessel Code, "Section III Case N-47-23" (ASME, New York, 1986).
2. F. MASUYAMA, "EPRI/National Power Conference on New Steels for Advanced Plant up to 620°C," edited by E. Metcalfe (Soc. Chem. Indus., London, 1995) p. 98.
3. A. ISETA, A. NATORI, Y. SAWARAGI, K. OGAWA, F. MASUYAMA and T. YOKOYAMA, *J. Therm. Nucl. Power, Jpn.* **45** (1994) 900.
4. F. ABE, M. IGARASHI, S. WANIKAWA, M. TABUCHI, T. ITAGAKI, K. KIMURA and K. YAMAGUCHI, "Parsons 2000 Advanced Materials for 21st Century Turbines and Power Plant," edited by A. Strang, W. M. Banks, R. D. Conroy, G. M. McColvin, J. C. Neal and S. Simpson (Cambridge, UK, 2000) p. 129.
5. "NRIM High-Temperature Low-Cycle Fatigue Data Sheets No.78" (National Research Institute for Metals, Tokyo, 1993).
6. "NRIM High-Temperature Low-Cycle Fatigue Data Sheets No. 62" (National Research Institute for Metals, Tokyo, 1989).
7. K. OHNO, K. DOZAKI, T. FUJIOKA, M. SUKEKAWA, K. TAGUCHI and H. KOTO, in Proceedings of the 73rd JSME Spring Annual Meeting, Chiba, Japan, April 1996 (JSME, Tokyo, 1996) p. 127.
8. S. NISHIJIMA, A. ISHII, K. KANAZAWA, S. MATSUOKA and C. MASUDA, in "Fundamental Fatigue Properties of JIS Steels for Machine Structural Use," NRIM Fatigue Data Sheet Technical Document, No.5 (National Research Institute for Metals, Tokyo, 1989).
9. Y. MURAKAMI, in "Metal Fatigue: Effects of Small Defects and Nonmetallic Inclusions" (Elsevier, Oxford, UK, 2002).

Received 15 July 2003
and accepted 29 April 2004